Electron Momentum Density of He and H_2; Compton X-Ray Scattering

P. Eisenberger
Bell Telephone Laboratories, Murray Hill, New Jersey 07974
(Received 14 May 1970)

The electron momentum density (EMD) of the electrons in the helium atom and hydrogen molecule were measured by Compton x-ray scattering. The results for helium, in both the liquid and gaseous state, are in agreement within the statistical accuracy of the experiment with Hartree-Fock calculations of the EMD. For the hydrogen molecule the effects of binding on the EMD are clearly observed. There is disagreement between Hartree-Fock calculations of the EMD for the hydrogen molecule and the measured EMD. This disagreement is attributed to non-Hartree-Fock electron-electron interaction effects, which are sizable in the H_2 molecule. In addition, for these systems, further proof of the validity of the impulse approximation is obtained by an accurate measurement of the Compton shift.

I. INTRODUCTION

The study of the electronic momentum density (EMD) by Compton x-ray scattering was initially proposed in 1929 by Dumond[1] and has recently been applied to numerous systems.[2-6] In 1937 Dumond[7] made a qualitative study of scattering from helium, but no quantitative comparison between theory and experiment was possible. In fact, in all the systems measured to date, no such quantitative comparison has been made because no truly simple system was accurately measured and no reliable theory for analyzing the results for scattering from bound electrons was available. Theoretical justification for the accuracy of the technique when scattering from weakly bound rather than free electrons has recently been given by Eisenberger and Platzman.[8] The results of that work will be briefly reviewed in Sec. II. The experimental results given in that work for liquid helium will be made quantitative and have been extended to include gaseous helium. Those results will be compared with theoretical calculations for helium performed by Hennecker[9] using Hartree-Fock self-consistent-field (HF-SCF) and multiconfiguration self-consistent-field (MC-SCF) wave functions. The agreement between theory and experiment will be seen to be within the experimental errors.

Experimental results on liquid and gaseous H_2 will be presented in Sec. IV after a description of the experiment is given in Sec. III. The H_2 results when viewed in the perspective of the accuracy of the He results will give the first strong evidence for the utility of the Compton x-ray scattering technique in discerning binding and electron-electron interaction effects. Those points will be discussed in Sec. IV where the experimental results will be compared with calculations performed by Henneker using HF-SCF and MC-SCF wave functions for H_2.

In Sec. V the advantages of the Compton (inelastic) scattering for probing wave functions over Rayleigh (elastic) scattering studies will be discussed. In the Appendix accurate measurements of the Compton shift for He and H_2 are described. They provide further evidence for the validity of the impulse approximation for weakly bound electrons.

II. GENERAL THEORY

The essential physical process which enables Compton x-ray scattering to provide information on the EMD is the doppler shifting of the scattered radiation due to the motion of the scattering electron. For a free moving electron, this is clearly illustrated by the conservation laws ($\hbar = 1$)

$$\vec{k} = \vec{k}_1 - \vec{k}_2 = \vec{p}_f - \vec{p}_0 , \tag{1a}$$

$$\omega = \omega_1 - \omega_2 = (p_f^2 - p_0^2)/2m = k^2/2m + (\vec{k}\cdot\vec{p}_0)/m , \tag{1b}$$

where (ω_1, ω_2) and (k_1, k_2) are the initial and final frequencies and wave vectors of the photon and (p_0, p_f) are the initial and final momenta of the electron.

Using the definitions

$$(\vec{k}_1\cdot\vec{k}_2)/|k_1||k_2| = \cos 2\theta_C ,$$

$$[(\vec{k}_1 - \vec{k}_2)\cdot\vec{p}_0]/|\vec{k}_1 - \vec{k}_2| = -q , \tag{2}$$

$$\lambda^* = (\lambda_1^2 + \lambda_2^2 - 2\lambda_1\lambda_2\cos 2\theta_C)^{1/2} ,$$

where λ_1, λ_2 are the initial and final wavelengths of the photon, one finds from Eq. (1) that (reinserting $\hbar$)

$$\lambda_2 = \lambda_1 + (2h/mc)\sin^2\theta_C + (q/mc)\lambda^* . \tag{3}$$

Equation (3) clearly shows that the wavelength of the scattered photon λ_2 depends linearly on the momentum projection q of the electron initial momentum $\vec{p}_0$ on the scattering vector $\vec{k}$. For q or $p = 0$ one obtains the well-known Compton shift

$$\lambda_2 - \lambda_1 = (2h/mc)\sin^2\theta_C . \tag{4}$$

Thus, to first order, the principle of the Compton scattering technique is to analyze the distribution of wave lengths λ_2 scattered from the sample in a fixed angle $2\theta_C$ and to relate that distribution to the distribution of q's of the electronic system.

Now, in general, the electrons of interest are not free and thus Eq. (1b) should be

$$\omega = \omega_1 - \omega_2 = |E_B| + p_f^2/2m , \tag{5}$$

where $|E_B|$ is the binding energy of the electron. The simplicity of Eqs. (1)–(3) is ruined, although the essential features are maintained.

For a hydrogenic system, the cross section for the Compton process is given by

$$\frac{d\sigma}{d\Omega d\omega} = \left(\frac{d\sigma}{d\Omega}\right)_{\mathrm{Th}} \frac{\omega_1}{\omega_2} \sum_f \sum_i |\langle f| e^{i\vec{k}\cdot\vec{r}} |i\rangle|^2 \times \delta(\omega - p_f^2/2m - E_B), \tag{6}$$

where $(d\sigma/d\Omega)_{\mathrm{Th}}$ is the Thomson cross section and $|f\rangle$ are the continuum hydrogenic final states. In deriving the impulse approximation, Eisenberger and Platzman[8] showed that to accuracy $2m|E_B|^2/k^2$, Eq. (6) could be rewritten as

$$\frac{d\sigma}{d\Omega d\omega} = \left(\frac{d\sigma}{d\Omega}\right)_{\mathrm{Th}} \frac{\omega_1}{\omega_2} \left(\frac{1}{2\pi}\right)^3 \int n(\vec{p}_0)\, d^3p_0 \times \delta(\omega - k^2/2m - k\cdot p_0/m), \tag{7}$$

where $n(\vec{p}_0)$ is the probability of an electron having momentum $\vec{p}_0$ and the δ function ensures that at each $\omega_2(\lambda_2)$ only those electrons with the right momentum projection to satisfy Eq. (3) will contribute to the integral. It is obvious that in the impulse approximation equation (7), the binding energy does not appear. This is the essence of the impulse approximation and is justified on physical grounds by asserting that the measurement is made sufficiently fast so that the potential in the ground and excited state of the atom is the same. For a general wave function $\psi(r)$ and atomic potential $V(r)$, the evaluation of Eq. (6) can only be done by numerical integration. Since $n(\vec{p}_0)$ is evaluated easily once $\psi(r)$ is known, Eq. (7) is calculated easily. It is for this reason that all previous experiments have compared their results with calculations based on the impulse approximation equation (7). For He and H_2, $2m|E_B|^2/k^2$ is 10^{-3}. Thus the impulse approximation can be used for analyzing the experimental results.

One can rewrite Eq. (7)

$$\frac{d\sigma}{d\Omega d\omega} = \left(\frac{d\sigma}{d\Omega}\right)_{\mathrm{Th}} \frac{\omega_1}{\omega_2} \frac{m}{|k|} J(q), \tag{8}$$

where

$$J(q) = \int_q^\infty n(\vec{p})\, dp_\alpha dp_\beta , \tag{9}$$

where p_α and p_β are perpendicular to q. $J(q)$ is the Compton profile and is the quantity which is used to compare theory and experiment. Note that for spherically symmetric systems it is deduced easily that

$$J(q) = 2\pi \int_q^\infty n(p_0) p_0\, dp_0 , \tag{10a}$$

$$\int_{-\infty}^{\infty} J(q)\, dq = 1 \text{ per electron} , \tag{10b}$$

$$I(p) = 4\pi p^2 n(p) = \left| 2q \frac{dJ}{dq} \right| . \tag{10c}$$

In the above, Eq. (10b) is just due to the normalization of $\psi(r)$ and in Eq. (10c) $I(p)$ is the EMD. Equations (8) and (10) will be used to analyze our results.

In the Appendix further proof is given for the validity of the impulse approximation through accurate measurements of the wavelength shift of the peak of the scattered distribution from the incident wavelength $(\lambda_2 - \lambda_1)$. Agreement is found with the free-electron results given in Eq. (4).

III. EXPERIMENT

The general experimental configuration is shown in Fig. 1. It closely parallels that used by Phillips and Weiss.[2] Molybdenum characteristic radiation was used in all these experiments. For both He and H_2 two separate measurements were made in the liquid state and one in the gaseous state. The measurements in the liquid were performed in a Dewar with separate pairs of input and exit beryllium windows 0.02 in. thick. The Compton angles $2\theta_C$ for the two measurements on the liquid were $133.7° \pm 2°$ and $141° \pm 2°$, respectively. For the gases a pressure cell was constructed with separate input and output beryllium windows 0.125 in. thick. Both gases were pressurized to 480 lb/in.^{2}. The Compton angle $2\theta_C$ was $170° \pm 7°$.

The Compton scattered radiation from He and H_2 was Bragg scattered from LiF (400) and analyzed into its wavelength components by relating the scattering angle to the wavelength by use of Bragg's law $(\lambda_2 = 2d \sin\theta_B)$. The spectrum was scanned repeatedly in an automatic fashion by stepping the LiF crystal in discrete steps through the range of scattering angles of interest. The system is capable of stepping $2\theta_B$ in increments of one thousandth of a degree. The smallest step taken in this study was four hundredths of a degree. This, together with stability studies of the Picker diffractometer, on which the LiF crystal was mounted, results in the conclusion that no significant error is introduced in the stepping process. Each spectrum reported in this work was swept on the order of 40–100 times in order to eliminate long-term drift. Peak counts accumulated varied from 48 000 to 10 000.

The raw data counts versus angle were converted in $J(q)$-versus-q Compton profiles in two distinct, though related, manners. Before describing the

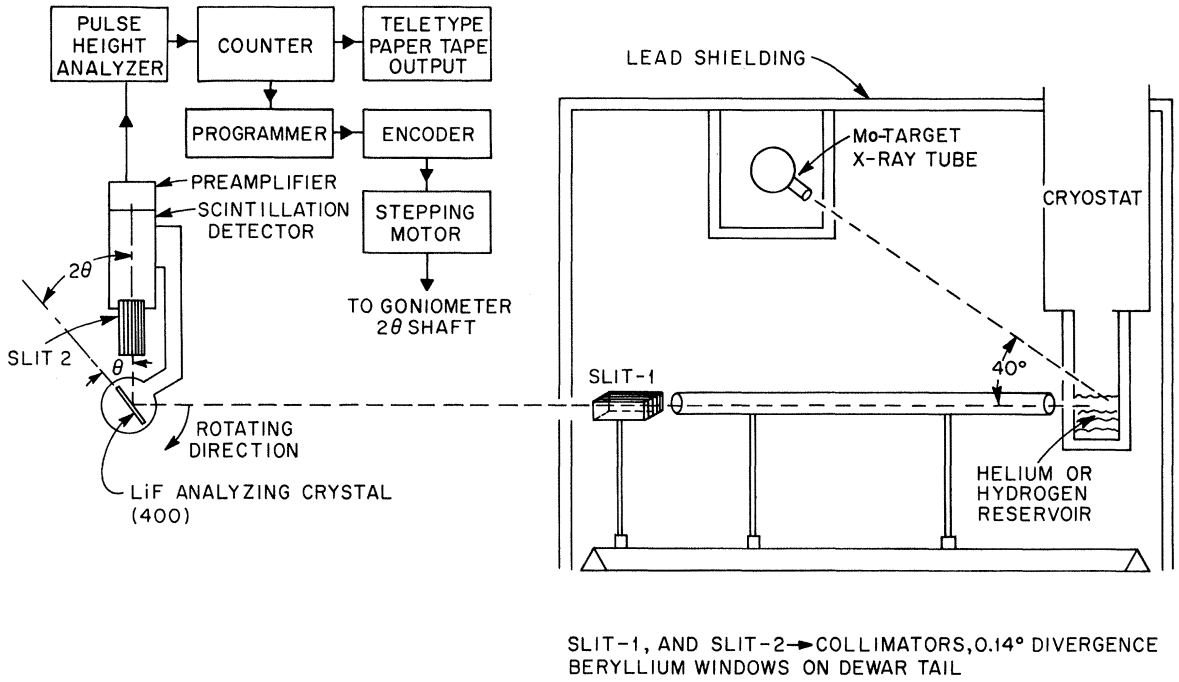

FIG. 1. Experimental configuration. For the gaseous experiments the Dewar was replaced by a pressure cell constructed with separate entrance and exit windows ($2\theta_C = 170.°$).

two methods, it should be pointed out that to measure the EMD only a relative measurement of the scattered intensity is necessary. Knowing the relative number of electrons with a given q, one can use the conservation condition of Eq. (10) to get the absolute values. Therefore, only relative corrections need be made, and they are very small over the small region of wavelength studied (0.73 to 0.77 Å). Corrections for absorption in the gases or liquids and beryllium windows were accounted for as well as the $(\omega_2/\omega_1)(1/|k|)$ prefactor in Eq. (8). The total corrections were taken to be zero at the peak, and were only 2–3% far in the tails.

In the first method the background was subtracted and then the Rachinger[10] separation was performed to eliminate the $K\alpha_2$ component. The resulting data were converted to counts versus q through Eq. (3) and then fitted with a function of the form

$$F(q) = \frac{1}{x_1 + x_2 q^2 + x_3 q^4 + x_4 q^6 + x_5 q^8 + x_6 q^{10} + x_7 q^{12}} \,. \tag{11}$$

The function $F(q)$ was then used in a trial-and-error convolution program in which the effects of finite resolution were removed. The form of the resolution function will be discussed shortly. The $J(q)$ was obtained by normalizing the result of the convolution so that it satisfied Eq. (10).

In the second approach, the raw data were fitted to a generalized function of $2\theta_B$. The corrections were made and then a Fourier-transform technique was used to remove both the effects of the $K\alpha_2$ component and finite resolution.[11] The resulting function of $2\theta_B$ was then converted into a function of q by Eq. (3) and normalized according to Eq. (10). Results of the two approaches to data analysis agreed within experimental error, though in speed and theoretical accuracy the Fourier technique is far superior.

As will be shown in Sec. IV, the largest resolution corrections are only on the order of 2% for He and 4% for H_2 and, therefore, though important in this study, they are not very large. Finite resolution comes essentially from two sources: The LiF crystal has finite wavelength resolution, and a finite input solid angle provides an uncertainty in the angle 2θ. From Eq. (3) it is easily seen that

$$\frac{dq}{d\lambda_2} = \frac{m_0 c}{\lambda^*} \,, \quad \frac{d\lambda_2}{\lambda_2} = \cot\theta_B \, d\theta_B \,, \tag{12a}$$

$$\frac{dq}{d\theta\, c} = \frac{4h}{\lambda^*} \sin\theta_C \cos\theta_C \,. \tag{12b}$$

The finite wavelength resolution was experimentally measured by scanning the molybdenum, $K\alpha_1$, and $K\alpha_2$ peaks. The wavelength resolution function was found to be essentially Gaussian with a slightly Lorenztian-like tail, but was taken to be a true Gaussian for the purposes of this study. Since the resolution corrections are only on the order of 2% for He and 4% for H_2, no significant error is intro-

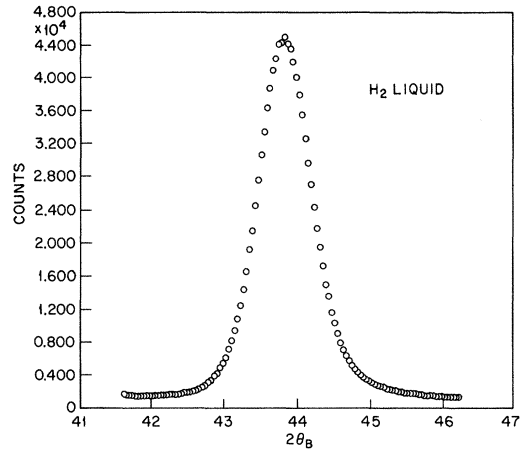

FIG. 2. Raw data for H_2 (liquid 2). Accumulated counts are plotted versus twice the Bragg angle ($2\theta_B$) of the LiF [400] crystal.

duced by this approximation. The variance of the distribution in q due to the distribution of wavelengths scattered at each $2\theta_B$ was different for each of the measurements because θ_B and λ^* in Eq. (12a) were different. However, the half-width for the distribution of Bragg angles $d\theta_B$ produced by the combined effect of the two collimators and LiF crystal was $\pm 0.05°$ for all experiments. The distribution of input solid angles was measured in a manner similar to that described in the Appendix and was found to be also essentially Gaussian. Again, the effective half-width in q was different in each experiment. The half-width for the distribution of scattering angles $d\theta_C$ was $\pm 1°$ for the liquid experiments and $\pm 3.5°$ in the gas experiments. The larger solid angle for the gas experiments does not introduce a substantial error because they were performed at $2\theta = 170°$, in which case $\cos\theta_C$ in Eq. (12b) is small. The wavelength uncertainty was the larger of the two sources of finite resolution. In reporting the results in Sec. IV, the effective variance σ used in the Gaussian resolution function will be given.

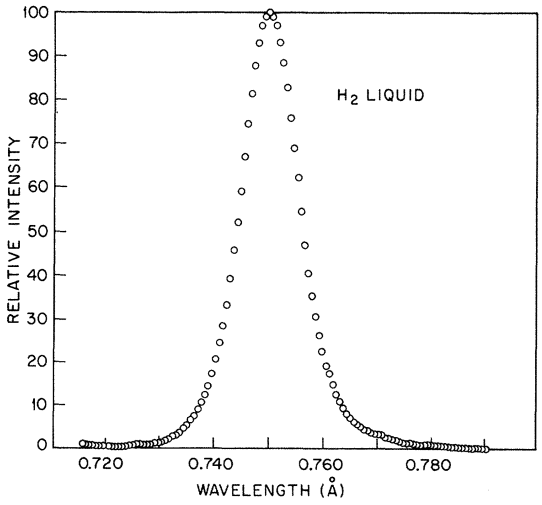

FIG. 3. H_2 (liquid 2), corrected data. The $K\alpha_2$ component has been removed by the Rachinger process, the background subtracted, and the corrections made.

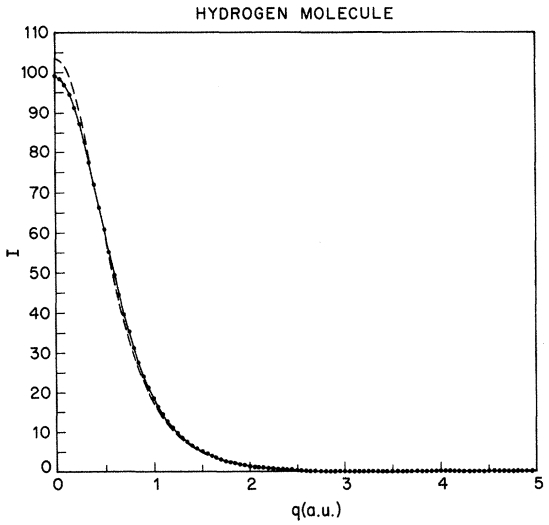

FIG. 4. H_2 (liquid 2), the effects of resolution. The • are the curve-fitted functions from Fig. 3. The dashed line is the best guess of the real function. The solid line is the result of convolving the best guess with the Gaussian resolution function. Note that the solid line is in good agreement with the •. Only one-half the curve is shown.

IV. EXPERIMENTAL RESULTS

For illustrative purposes Figs. 2–5 are presented. In Fig. 2 we show the raw data for liquid hydrogen. In Fig. 3 the $K\alpha_1$ and $K\alpha_2$ components have been separated by the Rachinger method and the separated data have been plotted. In Fig. 4 the effects of finite resolution are illustrated and in Fig. 5 the final normalized $J(q)$-versus-q curve is presented. As previously mentioned for both He and H_2, two runs were performed while in the liquid state and one in the gaseous state. In Tables I and II we have summarized the experimental results for He and H_2. Also given is the average result based on weighting the individual runs according to the square root of the peak counts accumulated in that run. The characteristic errors listed in the average column include contributions from statistical fluctuations and background and computational uncertainties. In particular, the background and computational uncertainties become very important in the tails of the Compton profile. The

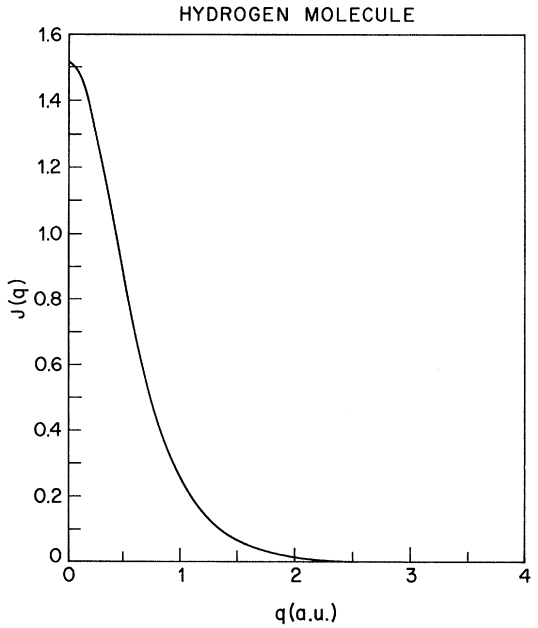

FIG. 5. H_2, the Compton profile. The resolution-corrected curve (dashed line Fig. 4) is normalized according to Eq. (10).

errors do not reflect any systematic corrections. The possible existence of systematic corrections is suggested by comparing the He and H_2 runs. It is easily noted that the deviations of the individual runs follows the same patterns for both He and H_2. Crudely speaking, the Compton profile for liquid 1 is narrower than results for liquid 2 and the gas. The helium runs could have been used as a standard to determine an ideal resolution function (i.e., one that gave the best agreement between theory and experiment). This resolution function then could have been used to analyze the H_2 data. However, since the deviations between runs are within the accuracy of the experiment, no correction for a possible systematic deviation was attempted. For the same reason no attempt has been made to distinguish the gas and liquid experimental results.

TABLE I. Experimental results for the Compton profile $J(q)$ for He. The q value is given in the first column with the $J(q)$ values for the three experiments listed in the first three columns and the weighted average given in the last column.

	He (Liq. 1)	He (Liq. 2)	He (Gas)	
$2\theta_C$	142°	133.7°	170°	
Peak counts	2×10^4	2×10^4	2×10^4	
σ (a.u.)	0.15	0.16	0.16	
0	1.071	1.068	1.058	1.066 (±0.7%)
0.1	1.057	1.053	1.047	1.052
0.2	1.017	1.011	1.009	1.012
0.3	0.955	0.951	0.956	0.954
0.4	0.877	0.872	0.879	0.876
0.5	0.789	0.786	0.803	0.789
0.6	0.697	0.696	0.710	0.700
0.7	0.608	0.608	0.620	0.612
0.8	0.524	0.524	0.532	0.527 (±1%)
0.9	0.448	0.447	0.449	0.448
1.0	0.381	0.383	0.381	0.382
1.2	0.273	0.281	0.272	0.275
1.4	0.196	0.200	0.190	0.195
1.6	0.141	0.144	0.127	0.137
1.8	0.102	0.100	0.092	0.098
2.0	0.074	0.069	0.059	0.067
2.5	0.030	0.025	0.026	0.027 (±10%)
3.0	0.010	0.007	0.007	0.008

TABLE II. Experimental results for the Compton profile $J(q)$ for H_2. The q value is given in the first column with $J(q)$ values for the three experiments listed in the first three columns and the weighted average given in the last column.

	H_2 (Liq. 1)	H_2 (Liq. 2)	H_2 (Gas)	
$2\theta_C$	142°	133.7°	170°	
Peak counts	10^4	4.8×10^4	2×10^4	
σ (a.u.)	0.15	0.16	0.16	Average
0	1.516	1.508	1.515	1.513 (±0.7%)
0.1	1.481	1.469	1.478	1.475
0.2	1.382	1.378	1.375	1.378
0.3	1.235	1.248	1.229	1.240
0.4	1.061	1.071	1.052	1.065
0.5	0.880	0.891	0.880	0.887
0.6	0.710	0.716	0.703	0.712 (±1%)
0.7	0.560	0.563	0.558	0.561
0.8	0.434	0.435	0.434	0.435
0.9	0.334	0.333	0.335	0.334
1.0	0.255	0.254	0.258	0.255
1.2	0.150	0.149	0.151	0.150 (±3%)
1.4	0.088	0.088	0.089	0.089
1.6	0.053	0.050	0.050	0.051
1.8	0.031	0.030	0.028	0.030 (±10%)
2.0	0.018	0.013	0.015	0.015

Theoretical calculations of the Compton profile are not in great abundance and, in fact, one of the secondary goals of this paper is to stimulate such calculations. The theoretical calculations presented in this work were performed by Henneker.[9] They were performed by using the basic relationship

$$J(q) = 2\pi \int_q^\infty \left| \int \psi(r)\, e^{-\vec{p}\cdot\vec{r}}\, d^3r \right|^2 p\, dp\,. \qquad (13)$$

For helium, two different wave functions $\psi(r)$ were used. The first came from Hartree-Fock self-consistent-field calculations of Clementi,[12] while the second came from multiconfigurational self-consistent-field (MC-SCF) calculations of Sabelli and Hinze.[13] The latter represent an improvement in the variational sense by resulting in a 0.0413-a.u. lower-energy state. The improvement results from the inclusion of non-Hartree-Fock correlation effects in the MC-SCF calculation. The results of the two calculations are given in Table III, where they are compared with the average of the three experiments on helium. It should be noted that the two calculations are almost identical, and that agreement with the experimental results is within the experimental error. The error is mainly

TABLE III. Comparison between theoretical (Ref. 9) and experimental Compton profiles for He.

q	He(HF-SCF) (Ref. 12)	He Experiment	He (MC-SCF) (Ref. 13)
0	1.0705	1.066 (±0.7%)	1.068
0.1	1.0568	1.052	1.055
0.2	1.017	1.012	1.015
0.3	0.955	0.954	0.954
0.4	0.878	0.876	0.876
0.5	0.791	0.789	0.788
0.6	0.700	0.700	0.698
0.7	0.611	0.612	0.609
0.8	0.527	0.527 (±1%)	0.525
0.9	0.450	0.448	0.449
1.0	0.382	0.382	0.381
1.2	0.271	0.275	0.271
1.4	0.190	0.195	0.191
1.6	0.134	0.137	0.135
1.8	0.095	0.098	0.096
2.0	0.068	0.067	0.069
2.5	0.031	0.027 (±10%)	0.031
3.0	0.015	0.008	0.015

statistical, except in the tails where the effects of the Rachinger separation and background dominate. This excellent quantitative agreement between theory and experiment for helium, which was previously qualitatively reported,[8] is the first such comparison between theory and experiment on a simple system.

Theoretical calculations for the H_2 molecule have also been made by Henneker.[9] To demonstrate the effects of binding, a calculation of $J(q)$ for two hydrogen atoms ($|E_B| = -1.0$ a.u.) was made. For the H_2 molecule itself a calculation of $J(q)$ based on HF-SCF[14] and MC-SCF[15] wave functions was also made. The latter calculation is not a very accurate attempt at evaluating the effects of non-Hartree-Fock electron-electron interactions but is included only to illustrate that those effects are large in H_2. For H_2, those interactions lower the binding energy from -1.133 to -1.174 a.u. The results of the three theoretical calculations are given in Table IV where they are compared to average experimental results obtained from Table II. In Fig. 6 the four results tabulated in Table IV are presented. It is clear that the effects of binding have been discerned; however, for the non-Hartree-Fock electron-electron corrections, the conclusions are more tenuous. As mentioned previously, the MC-SCF calculations are given to illustrate the possible size of the effects of Coulomb correlations on $J(q)$. Their actual calculation is not a simple matter.

It is well known that all the above calculations utilize the variational principle on the energy to calculate the wave function. It is also known that, even though one may approach very closely the lowest energy of the system, one may not have a wave function which can predict observables other than energy with any accuracy. It is in correcting this weakness of the variational approach that the Compton x-ray studies may be very useful. They have provided in H_2, and can provide in other molecules, a multivalued physical function $J(q)$ with which the variational wave function $\psi(r)$ can be checked and choices between different variational forms can be made. In this particular case the accuracy of the helium experiment strongly suggests that the variational wave function of H_2, chosen for the MCF calculation, is "worse" than the Hartree-Fock wave function, even though it produces a lower-energy state. In this context, "worse," of course, means with respect to a calculation of $J(q)$. The true $\psi(r)$ will be able to satisfy both observables.

The discrepancy between the experimental and theoretical results for H_2 suggests a reduction in low-momentum components (less than 0.3 a.u.) and an increase in the higher-momentum components. Such a change is what one would naively expect from the inclusion of non-Hartree-Fock electron-electron interaction effects. This is especially true for the case of H_2 when electron-electron interaction effects would be expected to enhance the p character of the molecule. For the same binding energy, the Compton profiles of p electrons are much broader than s electrons.

V. DISCUSSION

Experimental substantiation of the power of the Compton scattering probe has been obtained from quantitative comparison of experimental and theoretical Compton profiles. The experiments on H_2 strongly suggest that these studies will be of considerable use in deciding on the correct variational wave function. To substantiate this, it is hoped that the more sophisticated wave-function calcula-

TABLE IV. Comparison of theoretical (Ref. 9) and experimental Compton profile for H_2.

q	2H (Ref. 9)	H_2 (HF-SCF) (Ref. 14)	H_2 Experiment	H_2 (MC-SCF) (Ref. 15)
0	1.698	1.558	1.513 (±0.7%)	1.573
0.1	1.642	1.520	1.475	1.532
0.2	1.509	1.413	1.378	1.416
0.3	1.310	1.257	1.240	1.249
0.4	1.087	1.074	1.065	1.060
0.5	0.869	0.887	0.887	0.871
0.6	0.675	0.713	0.712 (±1%)	0.699
0.7	0.513	0.560	0.561	0.551
0.8	0.385	0.433	0.435	0.428
0.9	0.286	0.331	0.334	0.330
1.0	0.212	0.250	0.255	0.253
1.2	0.117	0.142	0.150 (±3%)	0.146
1.4	0.065	0.080	0.089	0.084
1.6	0.038	0.045	0.051	0.048
1.8	0.022	0.026	0.030 (±10%)	0.029
2.0	0.013	0.015	0.015	0.017

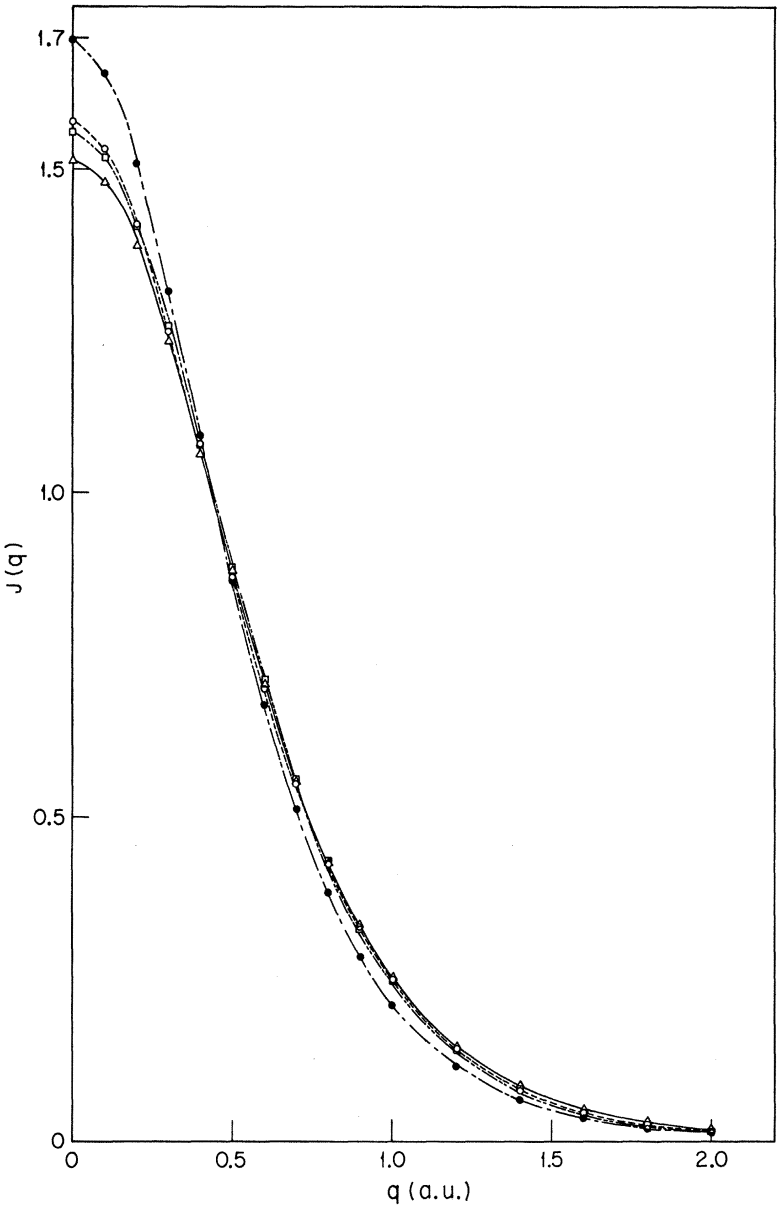

FIG. 6. Comparison of theory and experiment for H_2. Experiment ———; theory for two hydrogen atoms (2H) (Ref. 9) —— — ——; theory based on Hartree-Fock self-consistent-field (HF-SCF) wave functions (Ref. 14) —— -- ——; theory based on multiconfiguration self-consistent-field wave functions (Ref. 15) -------.

tions that Henneker is currently making will give good agreement with the experimental results. It is not unlikely that as the interplay between theory and experiment proceeds, greater experimental accuracy will be demanded as well as exact analysis of the data based on Eq. (6).

There is, in principle, no reason why this technique cannot be extended to other more complicated molecules. In fact, the author has already measured N_2, O_2, CH_4, and Ne, which will be reported in a subsequent publication. However, for those molecules the core electrons ($1s^2$) do not satisfy the impulse approximation and a more complicated analysis using Eq. (6) is required. From the study of neon we hope to ascertain the validity and accuracy of such an approach.

Both He and H_2 have been investigated via elastic scattering techniques.[16,17] There are three features which strongly favor the use of the Compton technique for studying wave functions. The first is that the Compton scattering experiment measures relative amplitudes over a small wavelength region and is, therefore, not plagued by the large experimental corrections which characterize elastic scattering studies. The second advantage concerns resolution capabilities. Compton studies are made under conditions of highest momentum transfer (backward scattering) whereas, by its very nature, elastic scattering studies of outer or weakly bound electrons involve small momentum transfers. In fact, Compton studies become easier for smaller wavelength and higher spatial resolution while the elastic

scattering studies are by the nature of the process limited to small momentum transfer. A final advantage of the Compton technique is its greater sensitivity to the wave function of the weakly bound electrons. In elastic scattering studies in the region of small momentum transfer, the core and outer electrons contribute equally. Thus for a high atomic-number atom, the outer electrons make a very small contribution to the scattered intensity. In the Compton technique, the situation is quite different. The deeply bound core electrons have a broad flat Compton profile as opposed to the outer electrons which have a sharp profile. Thus for an atom like potassium, the single 4*s* electron will account for approximately 33% of the scattered intensity near $q=0$ as opposed to 5% in elastic scattering studies. These three advantages should enable the Compton x-ray scattering probe to be very useful in measuring the EMD of outer electrons.

ACKNOWLEDGMENTS

The author is deeply thankful to B. Henneker for supplying calculations of $J(q)$ from existing wave functions. The cooperative spirit and generous help provided by R. Weiss in the early stages of this experiment is most gratefully acknowledged. The experimental and computational help of W. Marra was very useful. Discussions with P. M. Platzman concerning this manuscript were very helpful.

APPENDIX

The good agreement in helium between theory and experiment gives strong evidence for the validity of the impulse approximation. It is possible that even though the shape of the curve is correctly given by the impulse approximation, the kinematics it suggests is wrong. According to Ref. 8, the potential $V(r)$ which the electrons experience only affects the scattering dynamics to order $|E_B|^2/\hbar^2k^2/2m$, on the order of 10^{-3} for helium and hydrogen. That is, the Compton shift [Eq. (4)] should be changed by less than 0.1%. However, a crude scanning of Eqs. (5) and (6) would suggest that the Compton peak would be shifted by something on the order of the binding energy to shorter wavelengths. In fact, calculations by Bloch[18] and experiments by Ross and Kirkpatrick[19] would suggest that shifts in the wavelength of the Compton peak on the order of $|E_B|/\hbar\omega_1$ are to be expected. This would result in a decrease in the Compton shift of ~0.001 Å.

For hydrogen and helium, the Compton shifts were measured using, for both systems, the results labeled liquid 2. A schematic of the method used to measure the Compton angle $2\theta_C$ is shown in Fig. 7. The LiF crystal in the Dewar reflected the bremsstrahlung background in [400] and [600]. The LiF crystal mounted on the diffractometer analyzed the Bragg-scattered radiation in first order. The angle θ_C was determined by the relationship

$$\sin\theta_1 = \sin\theta_C = 3\sin\theta_2[600] = 2\sin\theta_2[400], \tag{A1}$$

where θ_1 and θ_2 are indicated in Fig. 7. The measurements were made before the H_2 run and after the helium run. The results for $\sin\theta_C$ were 0.919 67 ±0.0001 and 0.920 02 ±0.0003, respectively. Using the average of the two values, one finds $\sin\theta_C = 0.919\,89 \pm 0.0002$. Using that value in Eq. (4), one finds that $2h/mc\ \sin\theta_C = 0.04106 \pm 0.000\,02$ Å. The measured values were 0.04107 ±0.00 01 Å for H_2 and 0.041 50 ± 0.0003 Å for He. The H_2 run was much more accurate because of the larger number of counts accumulated and because it is almost 50% sharper than He.

In both cases the peak of the Compton profile was determined by fitting the experimental curves after corrections with a symmetric function of q. From the best-fit function the center was determined and

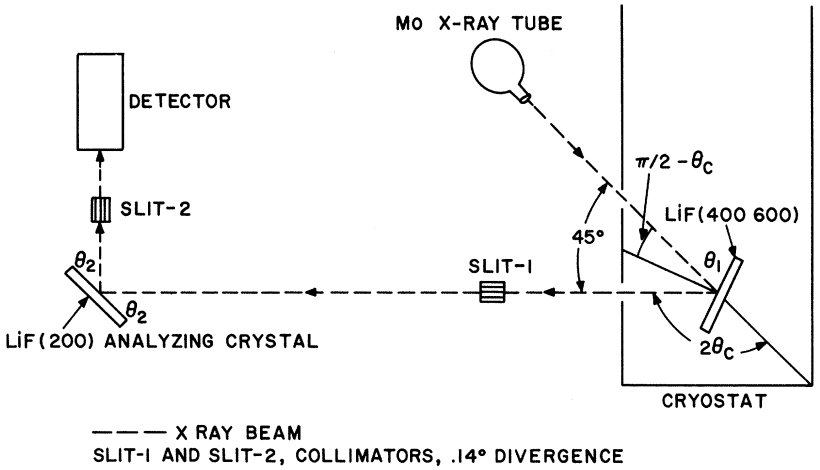

FIG. 7. Schematic diagram of technique used to measure $\sin\theta_C$.

it is this which was called the peak. Shifts on the order of the binding energy would have resulted in a Compton shift of 0.0401 Å, which is clearly not indicated by these studies.

[1]J. W. H. Dumond, Phys. Rev. 33, B643 (1929).
[2]W. Phillips and R. J. Weiss, Phys. Rev. 171, 790 (1968).
[3]M. Cooper and J. A. Leake, Phil. Mag. 15, 1201 (1967).
[4]R. J. Weiss and W. Phillips, Phys. Rev. 176, 900 (1968).
[5]A. Theodassious and P. Vosnidis, Phys. Rev. 145, B458 (1966).
[6]R. J. Weiss, Phys. Rev. Letters 24, 883 (1970).
[7]J. W. H. Dumond and H. A. Kirkpatrick, Phys. Rev. 52, 419 (1937).
[8]P. Eisenberger and P. Platzman, Phys. Rev. A 2, 415 (1970).
[9]B. Henneker (private communication).
[10]W. A. Rachinger, J. Sci. Instr. 25, 254 (1968).
[11]A. R. Stokes, Proc. Phys. Soc. (London) 61, 382 (1948).
[12]E. Clementi, IBM J. Res. Develop. Suppl. 9, 2 (1965).
[13]N. Sabelli and J. Hinze, J. Chem. Phys. 50, 648 (1969).
[14]P. Cade (private communication).
[15]A. C. Wahl and G. Das, J. Chem. Phys. 44, 87 (1966).
[16]D. Chip and L. O. Jennings, Phys. Rev. 132, B728 (1963).
[17]E. O. Wollan, Phys. Rev. 37, 862 (1931).
[18]F. Bloch, Phys. Rev. 45, 674 (1934).
[19]P. Kirkpatrick and P. A. Ross, Phys. Rev. 45, 667 (1934).

PHYSICAL REVIEW A VOLUME 2, NUMBER 5 NOVEMBER 1970

Ion Excitation of Characteristic X Rays for Elements with $72 \leqslant Z \leqslant 92$

P. B. Needham, Jr. and B. D. Sartwell
College Park Metallurgy Research Center, Bureau of Mines, U. S. Department of the Interior, College Park, Maryland 20740

A systematic study has been made of the ionization cross sections for ion excitation of the M-shell x rays of elements with Z in the region $72 \leq Z \leq 92$. Protons, H_2^+ ions, and α particles with incident energies ranging from 60 to 400 keV were used to excite the M lines of Hf, Ta, W, Au, Bi, and U. The Z dependence of the proton-excited x-ray yield for these elements, although differing sharply from previously published M-shell results, is shown to be consistent with the Z dependence for proton excitation of the K and L shells reported in earlier papers. Finally, we have compared the ionization cross sections of H_2^+ ions at incident energy E_0 with those for protons at incident energy $\frac{1}{2}E_0$, and found that within 30% they are in the ratio 2:1.

INTRODUCTION

The excitation of characteristic x rays from many solid materials by the impact of energetic ions has been extensively studied in recent years.[1-6] Previous publications have reported quite extensively on the K shells of low-Z elements and L shells of medium-Z elements, but little work has been reported on the excitation of M-shell x rays. Theoretical work has been restricted principally to calculation of K-shell and, to a lesser extent, L-shell ionization cross sections. The purpose of this paper is to present a systematic experimental study of the M-shell excitation of elements with $72 \leq Z \leq 92$ under bombardment by H^+, H_2^+, and He^{++} ions in the energy range 60–400 keV.

The calculations of the K-shell ionization cross sections by Henneberg[7] and Huus,[8] and later by Merzbacher and Lewis,[9] remain as the principal theoretical works. These calculations utilized a Bethe-Born approximation, using plane wave functions for the incident projectile and unperturbed atomic wave functions for the electrons to be ejected from the target atom during the collision process. The failure of this approach for protons at low (< 200 keV) energies resulted in the use of relativistic wave functions for the K-shell electrons by Jamnik and Zupancic.[10] The relativistic corrections proved to be significant only for high-Z elements and still failed to provide good agreement with experimental measurements. A semiclassical time-dependent perturbation method was used by Bang and Hansteen,[11] in which the deflection of the projectile in the Coulomb field of the nucleus of the target atom was shown to be significant for projectiles incident at low energies. However, these corrections failed to match known experimental results for protons below 150 keV.

Recently, Brandt *et al.*[12] considered the effects of the binding of the K electrons of the target atom